Supporting Information

Quasi physisorptive two dimensional tungsten oxide nanosheets with ultra sensitivity and selectivity to NO_2

Hareem Khan,[a] Ali Zavabeti,[a] Yichao Wang,[b] Christopher J. Harrison,[a] Benjamin J. Carey,[a] Md Mohiuddin,[a] Adam Chrimes,[a] Isabela Alves De Castro,[a] Bao Yue Zhang,[a] Ylias M. Sabri,[c] Suresh K. Bhargava,[c] Jian Zhen Ou,[a] Torben Daeneke,[a] Salvy P. Russo,[d,*] Yongxiang Li[a] and Kourosh Kalantar-zadeh[a,*]

[a] School of Engineering, RMIT University, 124 La Trobe Street, Melbourne, Victoria, 3000, Australia
[b] School of Life and Environmental Sciences, Deakin University, Waurn Ponds, Victoria, 3216, Australia
[c] Centre for Advanced Materials and Industrial Chemistry (CAMIC), School of Science, RMIT University, Melbourne, Victoria, 3000, Australia
[d] School of Applied Sciences, RMIT University, Melbourne, Victoria, 3000, Australia

[*]E-mail: kourosh.kalantar@rmit.edu.au and salvy.russo@rmit.edu.au

Table S1 Reports on some 2D tungsten oxide fabrication methods and their advantage

Synthesis method	Comparison	Ref
Chemical vapour deposition (CVD)	Conformal film but requires elevated temperatures, releases toxic by-products and has restrictive operating conditions	[1]
Hydrothermal	Effective for large-scale and controllable synthesis but uses expensive autoclaves	[2-4]
Liquid synthesis e.g. anodization and acid etching	Low-cost, fast, tunable but may require dangerous reagents	[5-7]
Sol-gel	Simple, inexpensive and controllable but end-product may contain contain impurities that degrade optical and electrical properties of the material	[8]
Exfoliation	Control over structure, fast and use fewer chemicals but has low yield	[9, 10]
Wet-chemical and sonication	Low-cost, facile, suitable for mass production due to good yield	This work

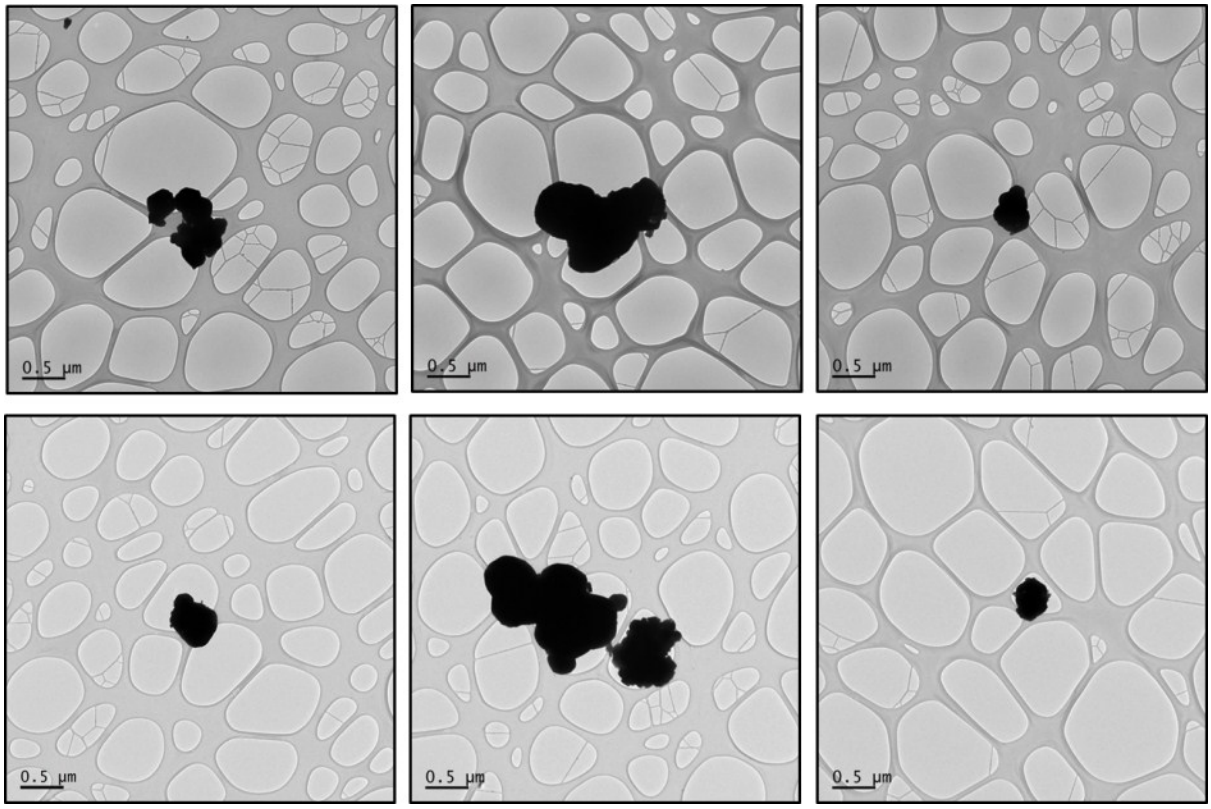

Fig. S1 TEM images of preparatory tungsten particles of size 0.5 µm.

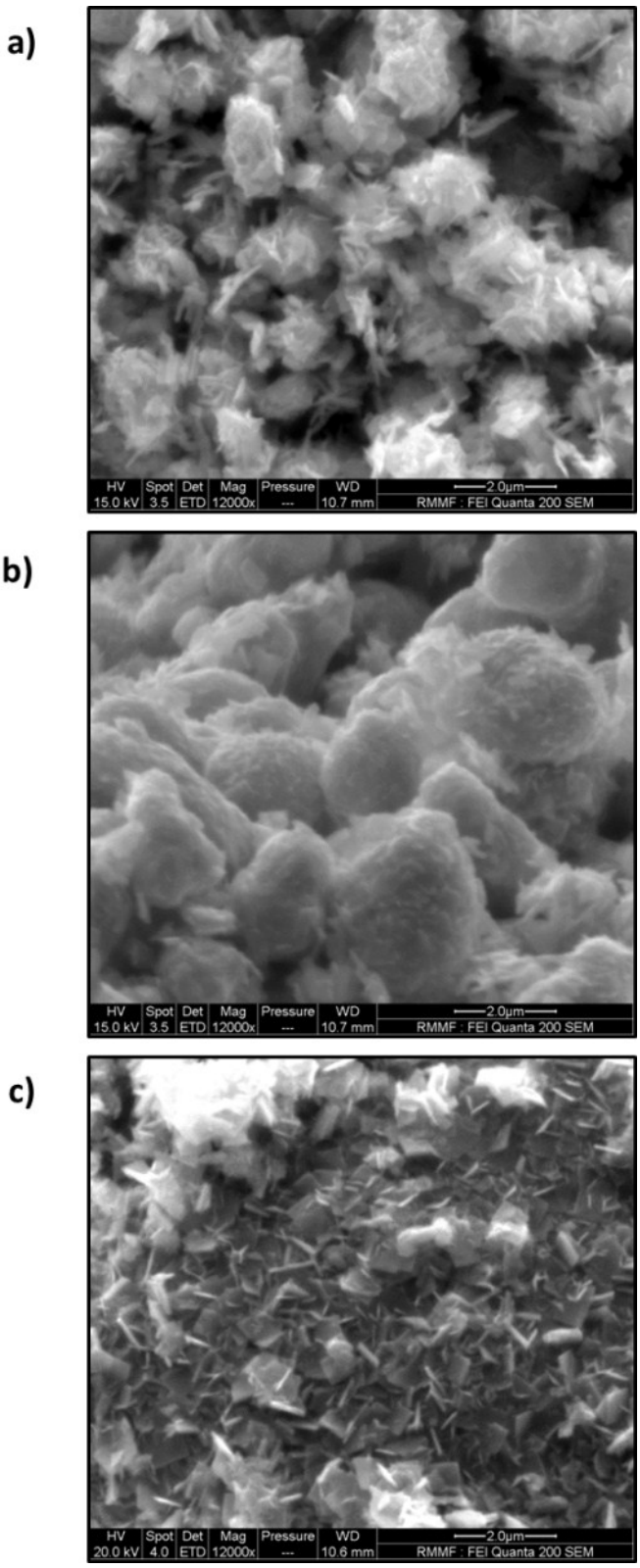

Fig. S2 SEM images of the unannealed samples synthesised with various sizes of tungsten particles: a) 0.5 µm b) 5 µm c) 40 µm

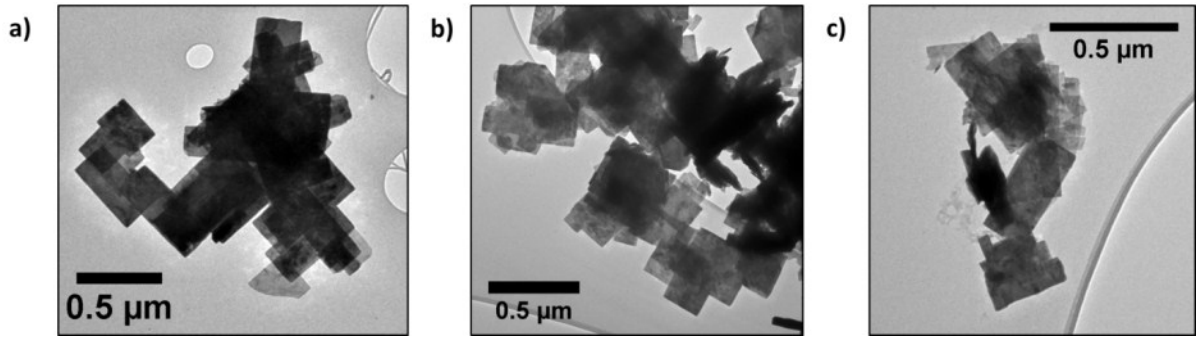

Fig. S3 TEM images of samples made from different sized tungsten particles: a) 0.5 µm b) 5 µm and c) 40 µm

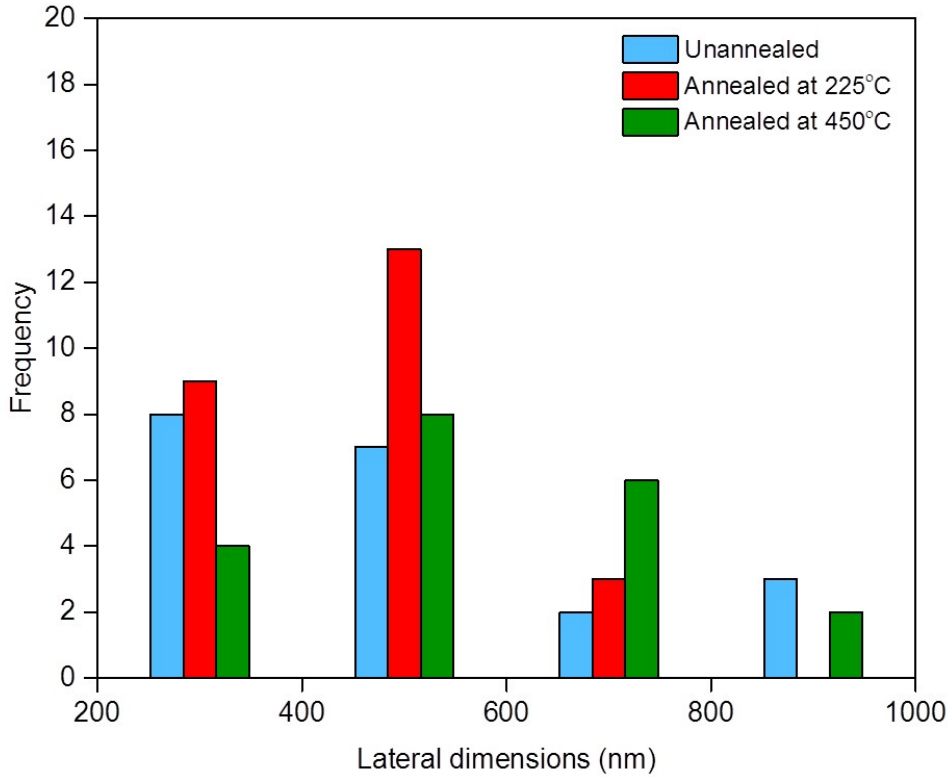

Fig. S4 Statistical analysis of nanosheet lateral dimensions seen in TEM images. Generated from 50 sheets each.

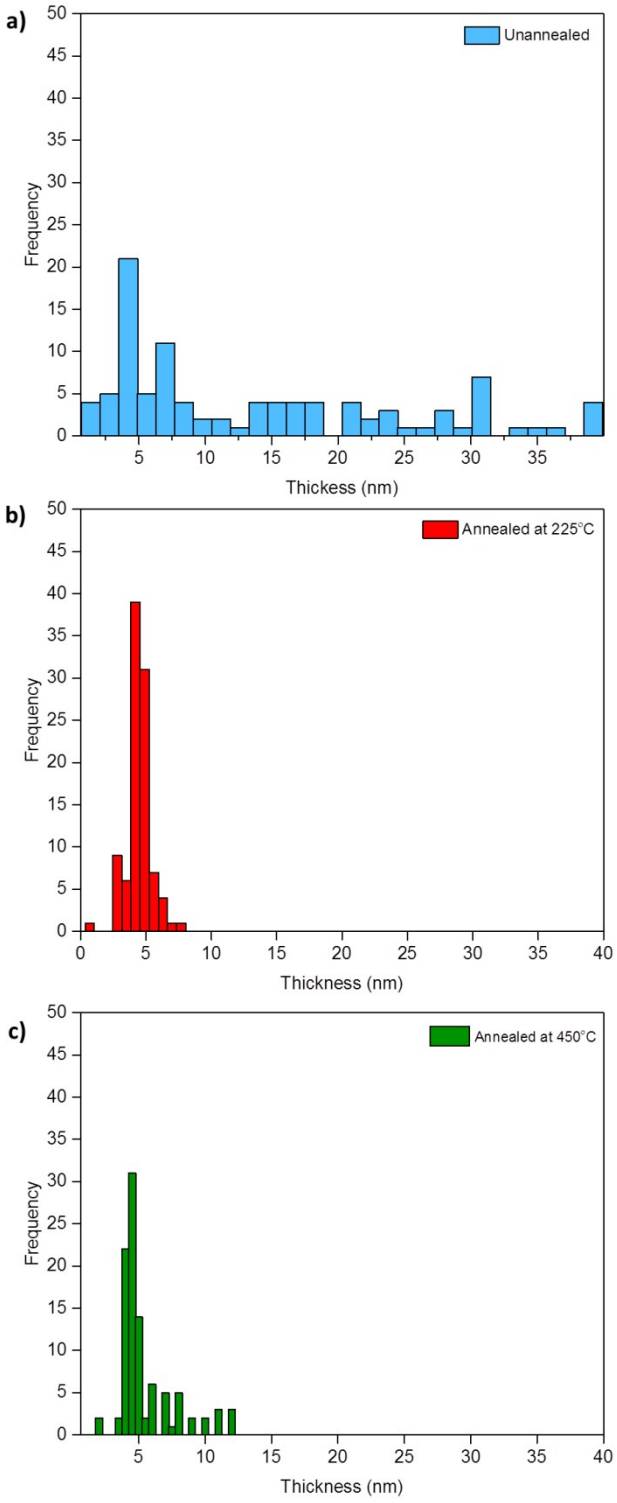

Fig. S5 Statistical analysis of nanosheet thicknesses as seen in AFM distributions images. 100 sheets were counted per sample

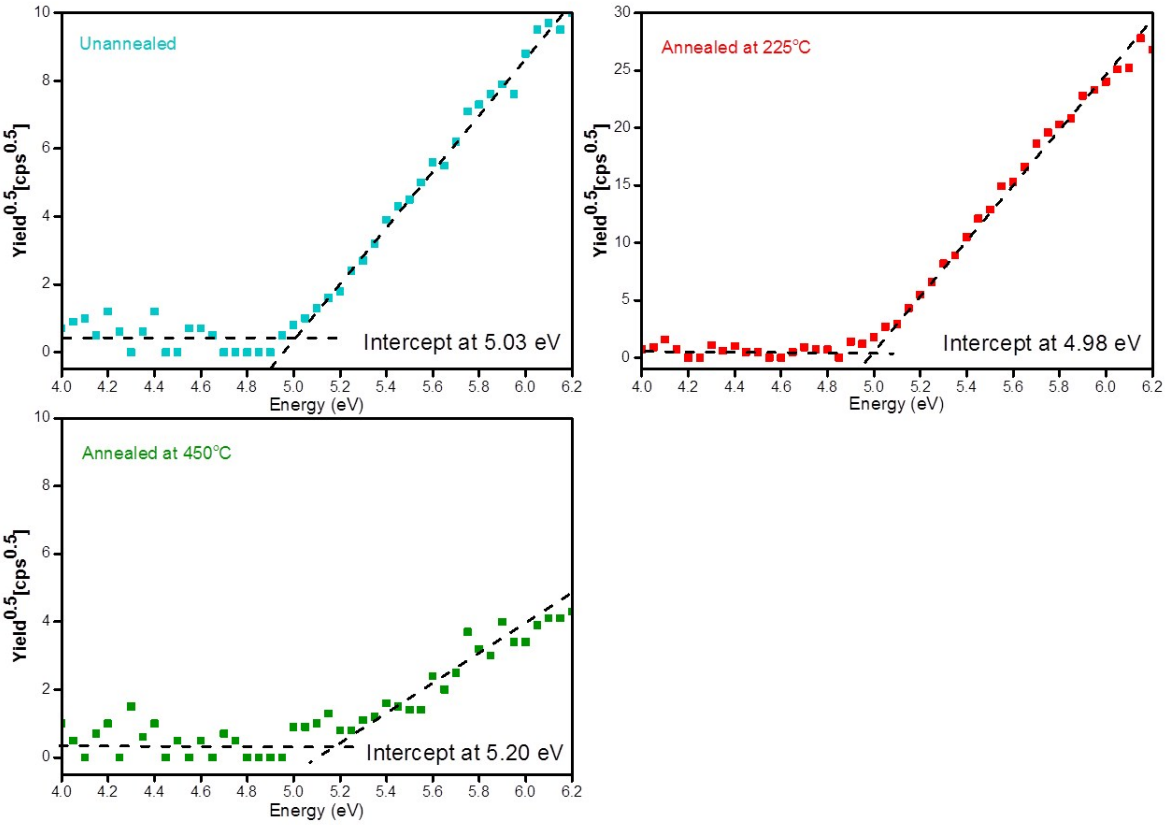

Fig. S6 PESA spectra of the samples- unannealed, annealed at 225◦C and annealed at 450◦C

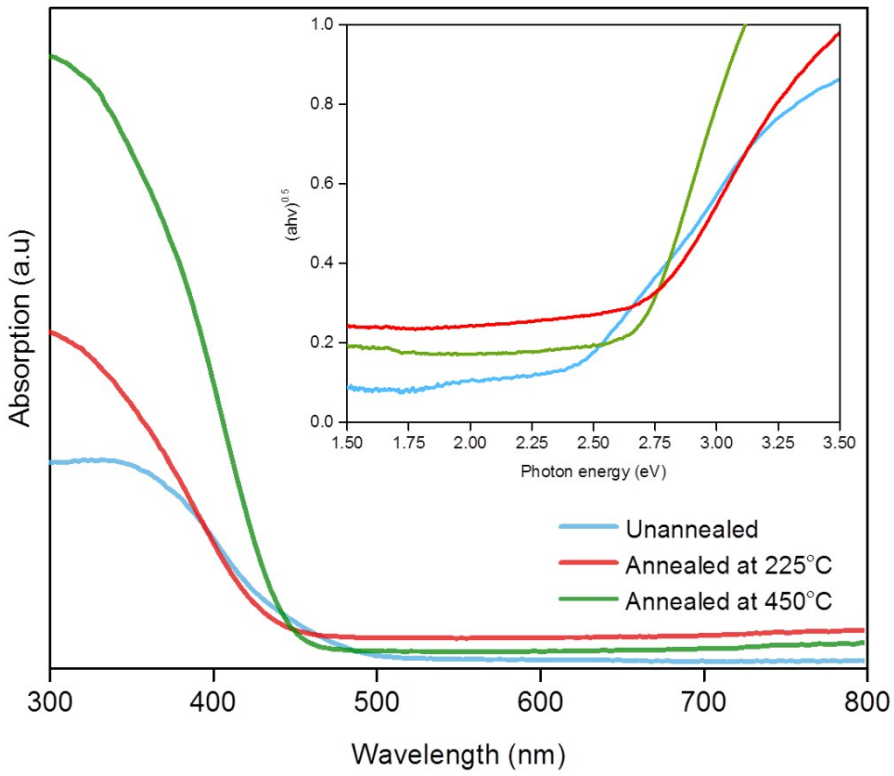

Fig. S7 UV-Vis spectra, with inset of Tauc plots plotted for samples: unannealed, annealed at 225◦C, and annealed at 450◦C

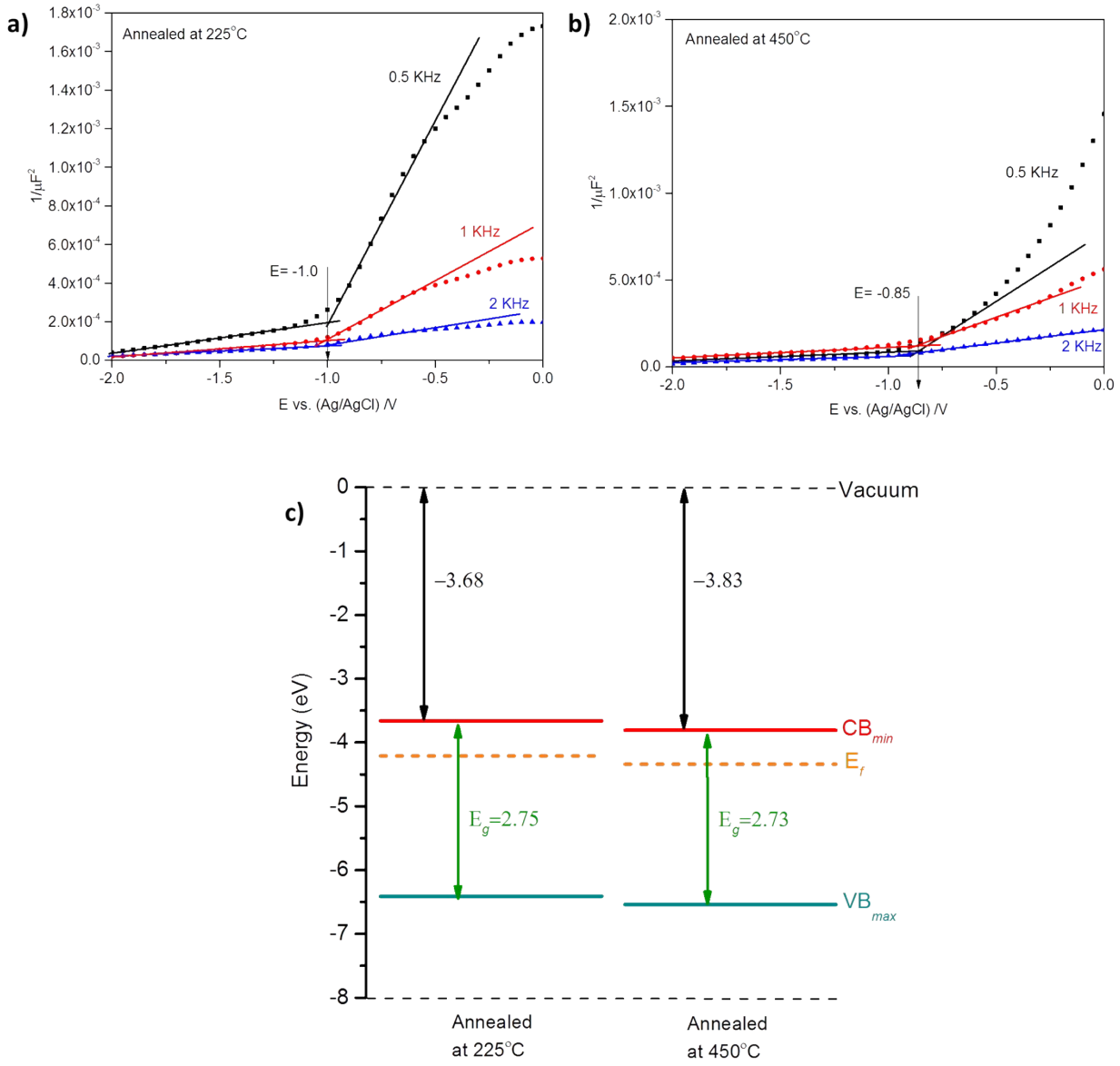

Fig. S8 Mott-Schottky plots measured for the two samples used for gas-sensing a) annealed at 225°C and b) annealed at 450°C. The samples were dropcasted onto carbon paper which was used as a working electrode. The active area was approximately 1 cm^2. A freshly calibrated Ag/AgCl reference electrode was utilised. The counter electrode was a carbon rod. Mott-Schottky plots were collected using sinusoidal signal at frequencies of 0.5, 1 and 2 kHz at 5 mV amplitude. c) the resulting band diagram using conduction band from Mott-Schottky, band-gap from Tauc plots and the valence band value from the XPS valence spectra.

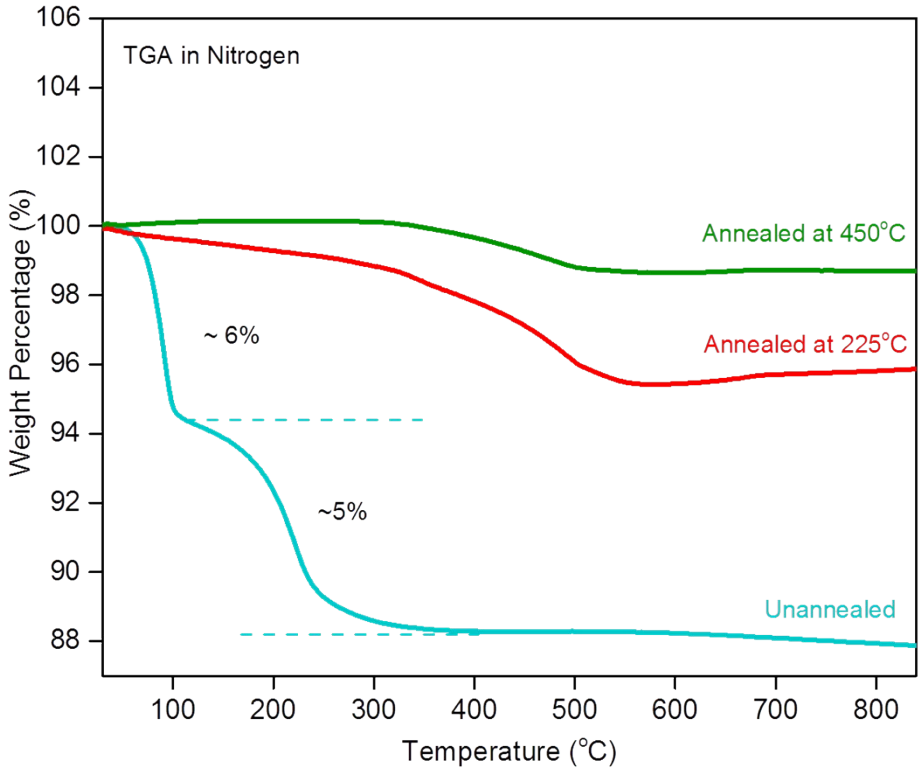

Fig. S9 TGA of the samples (unannealed, annealed at 225◦C and annealed at 450◦C) in Nitrogen between 30◦C- 850◦C at 20◦C min $^{-1}$

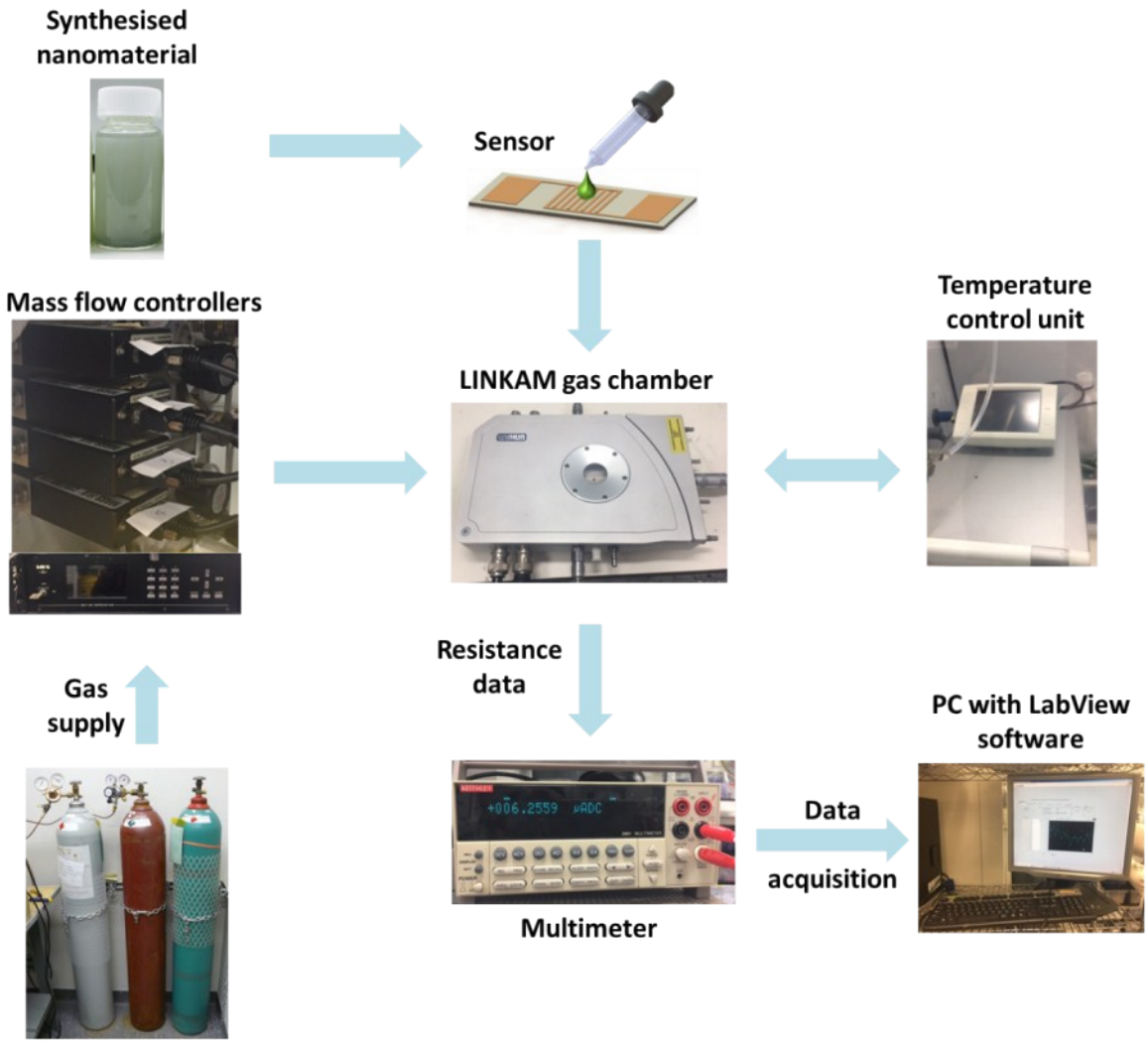

Fig. S10 Gas-sensing measurement set-up

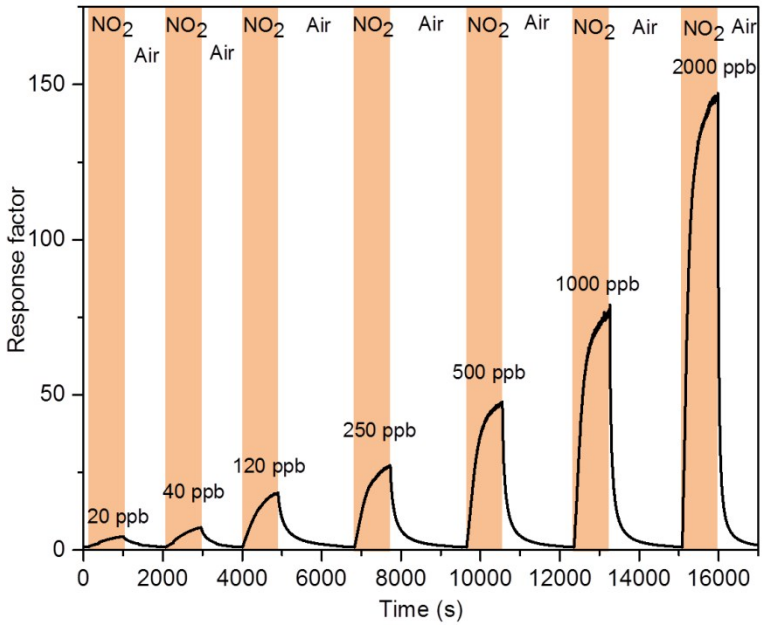

Fig. S11 Dynamic response of sample annealed at 450°C to different concentrations at 150°C.

Table S2 Gas sensing performance of the gas sensors with material annealed at 225°C and 450°C to 40 ppb at different operating temperatures

Operating temperature [°C]	Annealed at 225°C			Annealed at 450°C		
	Response factor	Response time [s]	Recovery time [s]	Response factor	Response time [s]	Recovery time [s]
100	-	-	-	2.2	836	1000
125	-	-	-	3.0	813	678
150	29.3	485	155	7.3	736	519
175	7.7	585	136	8.4	790	415
200	1.0	500	125	7.0	700	400

- This indicates that the values were unmeasurable by the multimeter due to drift or due to values being beyond the measurement capability of the instrument.

Table S3 Dynamic gas sensing performance of the gas sensors with material annealed at 225°C and 450°C to different concentrations of NO_2 at 150°C operating temperature

Concentration [ppb]	225°C annealed			450°C annealed		
	Response factor	Response time [s]	Recovery time [s]	Response factor	Response time [s]	Recovery time [s]
20	15.5	413	250	4.4	750	672
40	29.3	485	155	7.3	736	519
120	66.2	286	138	18.4	657	752
250	-	-	-	27.2	628	546
500	-	-	-	47.8	548	380
1000	-	-	-	76.3	477	280
2000	-	-	-	147.2	450	162

- This indicates that the values were unmeasurable by the multimeter due to drift or due to values being beyond the measurement capability of the instrument.

Table S4 Gas sensing performance of the sensors with material annealed at 225°C and 450°C to different gases at 150°C and the resistance trend

Gas	225°C annealed		450°C annealed	
	Response factor	Resistance trend	Response factor	Resistance trend
NO_2 (40 ppb)	29.3	↑	7.3	↑
NH_3 (1200 ppm)	1.3	↓	1.7	↓
H_2S (1 ppm)	1.5	↓	1.3	↓
CO_2 (10%)	1.0	↓	1.1	↑
H_2 (0.5%)	1.1	↑	1.1	↑
Humidity (50%)	1.0	↑	1.2	↑

↑ indicates that the resistance of the material increases when exposed to the specified gas
↓ indicates that the resistance of the material decreases when exposed to the specified gas

Table S5 The calculated molecule-surface adsorption energies of 2D tungsten oxide nanosheets toward H_2, CO_2, H_2S, NH_3, and NO_2 at T= 423K

Molecules	Binding energy (eV)
NO_2	-0.31
NH_3	-0.11
H_2S	-0.08
CO_2	0.11
H_2	-0.04

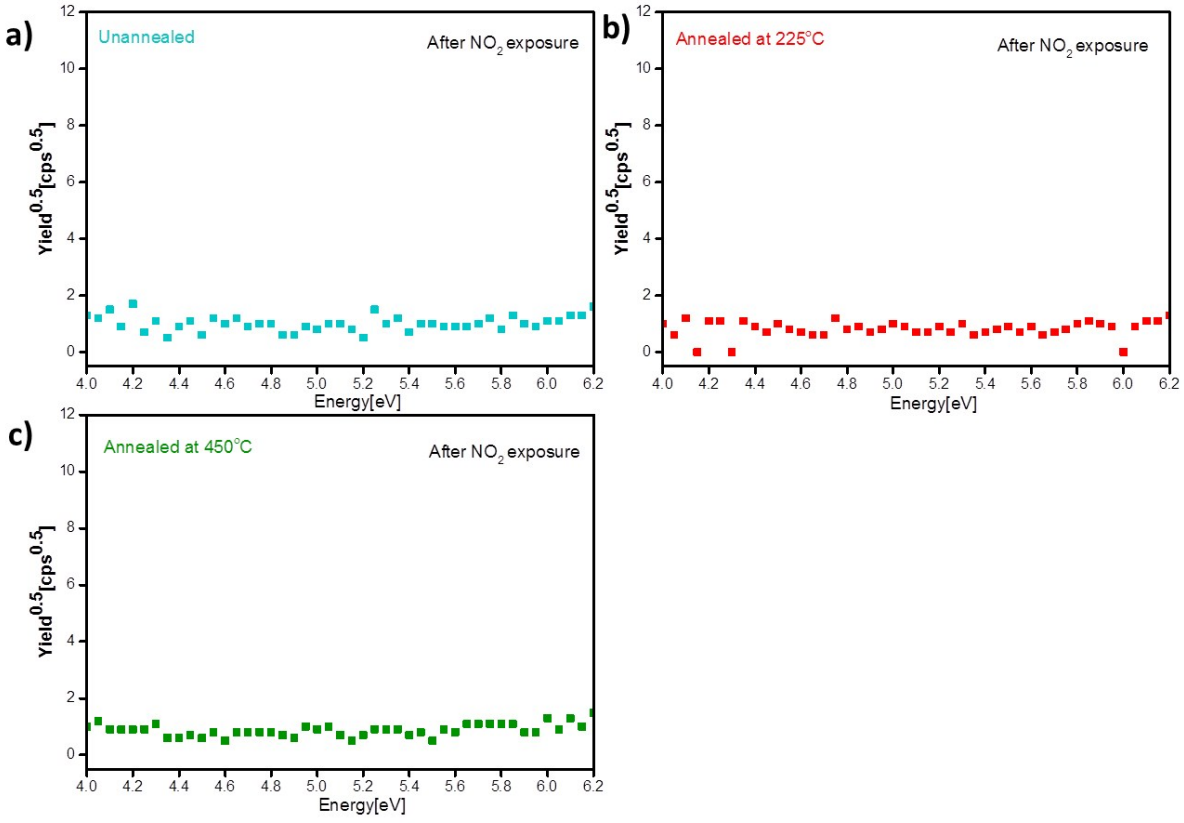

Fig. S12 PESA spectra after exposure to NO_2 gas showing Fermi levels shift beyond measurement capability of instrument at 6.2 eV for samples: a) unannealed b) sample annealed at 225°C and c) 450°C

References

1. R. G. Palgrave and I. P. Parkin, *Journal of Materials Chemistry*, 2004, **14**, 2864-2867.
2. T. Kida, A. Nishiyama, Z. Hua, K. Suematsu, M. Yuasa and K. Shimanoe, *Langmuir*, 2014, **30**, 2571-2579.
3. X. Han, X. Han, L. Li and C. Wang, *New Journal of Chemistry*, 2012, **36**, 2205-2208.
4. X. Gao, X. Su, C. Yang, F. Xiao, J. Wang, X. Cao, S. Wang and L. Zhang, *Sensors and Actuators B: Chemical*, 2013, **181**, 537-543.
5. A. Z. Sadek, H. Zheng, M. Breedon, V. Bansal, S. K. Bhargava, K. Latham, J. Zhu, L. Yu, Z. Hu, P. G. Spizzirri, W. Wlodarski and K. Kalantar-zadeh, *Langmuir*, 2009, **25**, 9545-9551.
6. J. Z. Ou, M. H. Yaacob, J. L. Campbell, M. Breedon, K. Kalantar-zadeh and W. Wlodarski, *Sensors and Actuators B: Chemical*, 2012, **166**, 1-6.
7. E. Widenkvist, R. A. Quinlan, B. C. Holloway, H. Grennberg and U. Jansson, *Crystal Growth and Design*, 2008, **8**, 3750-3753.
8. M. Breedon, P. Spizzirri, M. Taylor, J. du Plessis, D. McCulloch, J. Zhu, L. Yu, Z. Hu, C. Rix, W. Wlodarski and K. Kalantar-zadeh, *Crystal Growth & Design*, 2010, **10**, 430-439.
9. K. Kalantar-zadeh, A. Vijayaraghavan, M.-H. Ham, H. Zheng, M. Breedon and M. S. Strano, *Chemistry of Materials*, 2010, **22**, 5660-5666.
10. J. Yan, T. Wang, G. Wu, W. Dai, N. Guan, L. Li and J. Gong, *Advanced Materials*, 2015, **27**, 1580-1586.